COMMUNICATION

A Simple Approach to Boost Capacitance: Flexible Supercapacitors Based on Manganese Oxides@MOFs via Chemically Induced In Situ Self-Transformation

Yi-Zhou Zhang, Tao Cheng, Yang Wang, Wen-Yong Lai,* Huan Pang,* and Wei Huang*

Energy storage has become a scientific and technological issue no less important than energy production, the two of which together power the modern human society in an eco-friendly way.[1] Efficient energy storage is particularly important in the context of flexible electronics—a research area that is about to change our everyday life,[2,3] where flexible energy storage has become the bottleneck of the performance improvement of flexible electronic systems.[4,5] Supercapacitors (SCs, also known as electrochemical capacitors) as an important class of electrochemical energy storage devices (the others include batteries, fuel cells, etc.) hold an important and unique position that bridges the gap between conventional capacitors and batteries in terms of energy density and power density.[6–8] Owing to their superior qualities such as long lifespan and high power output, which are important for flexible/wearable applications, SCs have received considerable and growing interest in the recent decade.[9]

There are mainly two kinds of SCs depending on the charge storage mechanisms: The electrical double layer capacitors (EDLCs), where electrochemical energy is stored by ion adsorbing–dislodging, and pseudocapacitors, where capacitance comes from fast surface redox reactions.[10,11] EDLCs mainly utilize carbon materials (activated carbon, carbon nanotubes, graphene) as the electrode materials, while pseudocapacitors mostly use transition metal oxides and conducting polymers.[12–14] The search for the optimal electrode materials

fuels the development of SCs. The combination of the two charge storage mechanisms has shown its promise in many electrode systems for providing us with the optimal electrode materials.[15–17]

Metal-organic frameworks (MOFs) are a class of highly porous materials in which metal ions or clusters are coordinated by organic ligands. Since the 1990s,[18] they have found wide application in fields such as gas storage/separation[19] and catalysis,[20,21] drug delivery,[22] imaging and sensing,[23,24] etc. The exceptionally large surface area and variable sites for redox reactions of MOFs make them intrinsically suitable as electrode materials for electrochemical energy storage devices like batteries[25] and more recently SCs. MOFs' application potential for SCs has not been exploited until merely a decade ago.[26] So far, SC electrodes based on MOFs are mostly fabricated via two general approaches: 1) MOFs are mainly used as sacrificial templates to afford porous carbon,[27–29] doped carbon,[30] metal oxides[31] or composite materials like metal oxide-carbon (MO-C).[32] 2) MOFs have also been used directly as SC electrode materials, although not until very recently.[33] Of the two approaches, the template approach has received more attention so far, however the high temperature treatment will inevitably increase the cost, and the intricate porous structure of MOFs cannot be well utilized. Thus, the second approach as demonstrated in the pioneering work by Yaghi and co-workers in 2014 seems very promising.[33] The potential of MOFs for the supercapacitor electrode application mainly originate from the exceptionally large surface area and porous inner structure: Electrolyte ions can easily diffuse through the micro/mesopores of the frameworks, resulting in large EDLC type capacitance.

MOFs' direct application as SC electrode materials has mainly encountered two problems: Most MOFs lack sufficient electrical conductivity and mechanical/chemical stability. The capacitance of MOFs is generally low because the EDLC type capacitance is much smaller than the pseudocapacitance. The low conductivity and stability problem can be overcome by choosing a MOF with high conductivity and stability, adding additives, or making composites between MOFs and conductive carbon materials like graphene.[34] On the other hand, the capacitance problem is more interesting because ingenious addition of pseudo-capacitance can make a big difference in the electrochemical performance of MOF-based electrodes. Actually, MOFs usually possess some pseudocapacitance due to the valence variability of the metallic ions that can act as redox centers, however, it is far more effective to add pseudocapacitance by introducing pseudocapacitive materials into the MOF systems. Metal oxides and conductive polymers are the most commonly used pseudocapacitive materials. As an example,

Y.-Z. Zhang, T. Cheng, Y. Wang, Prof. W.-Y. Lai, Prof. W. Huang
Key Laboratory for Organic Electronics and Information Displays (KLOEID) and Institute of Advanced Materials (IAM)
Jiangsu National Synergetic Innovation Center for Advanced Materials (SICAM)
Nanjing University of Posts and Telecommunications
9 Wenyuan Road, Nanjing 210023, China
E-mail: iamwylai@njupt.edu.cn; wei-huang@njtech.edu.cn

Prof. H. Pang
College of Chemistry and Chemical Engineering
Yangzhou University
Yangzhou 225002, China
E-mail: huanpangchem@hotmail.com

Prof. W.-Y. Lai, Prof. W. Huang
Key Laboratory of Flexible Electronics (KLOFE) and Institute of Advanced Materials (IAM)
Jiangsu National Synergetic Innovation Center for Advanced Materials (SICAM)
Nanjing Tech University (NanjingTech)
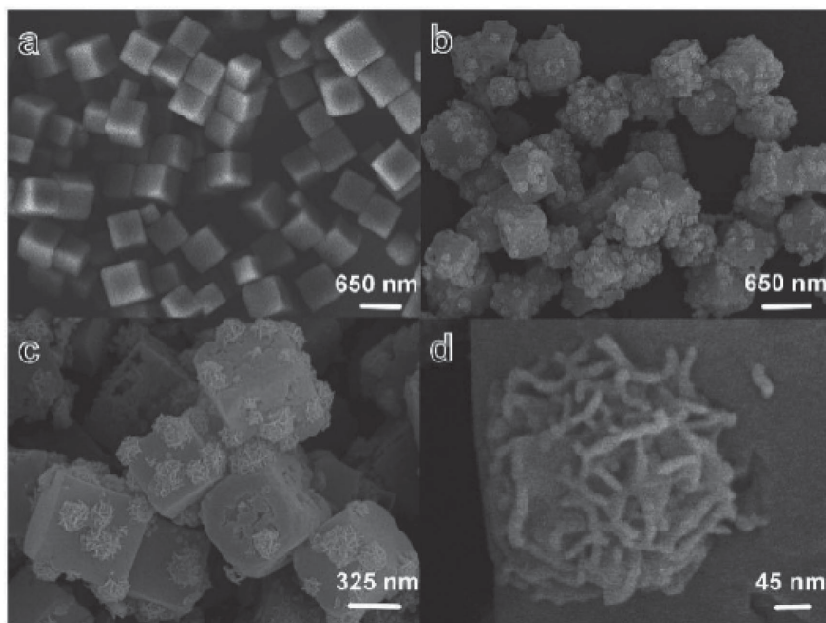30 South Puzhu Road, Nanjing 211816, China

Figure 1. SEM images of a) MHCF and b–d) MnOx–MHCF at different magnifications.

Chen and Wang used electrodeposition to deposit MnO_2 on a Ni-based MOF, resulting in a $NiHCF@MnO_2$ dual layer structure.[35] The dual-layer-electrode showed ≈26% increase in terms of specific capacitance (244 F g^{-1} $NiHCF@MnO_2$ vs 177.5 F g^{-1} NiHCF).[35] Wang et al. extended this method to make electrode materials for flexible SCs. They endowed a MOF-based electrode with a much higher capacitance as well as a higher conductivity by electrochemically interweaving MOF crystals with polyaniline.[36] However, the electrochemical deposition method is instrument dependent, more importantly, the dual layer structure resulting from this approach cannot unleash the full potential of the synergistic effect between the two constituent materials.[35]

Our assumption is that by making more intimate connection between the pseudocapacitive materials and MOFs, the performance of the composite can be significantly increased. In this report, we introduce metal oxides into the MOF systems through a very simple one-step chemically induced self-transformation process. The reaction is fast (less than 20 min), the reactant (NH_4F) is cheap, and no sophisticated equipment is needed. The process resulted in threefold increase in terms of specific capacitance compared to the pristine MOF (≈1200 F g^{-1} vs ≈300 F g^{-1} at 10 A g^{-1}) due to the more intimate connection between the pseudocapacitive manganese oxide and MOFs. Our approach is unique in that the pseudocapacitive elements come from the in situ growth of manganese oxides from the Mn-containing MOF itself in response to the addition of NH_4F, rather than from the outside environment. Specifically, MOF–manganese hexacyanoferrate hydrate (MHCF) nanocubes were selected as the starting materials because of their high performance as supercapacitor electrodes.[37] By adding NH_4F, the manganese in the framework grew into manganese oxides with the shape of "nanoflowers", decorating the surfaces of the smooth MHCF cubes. The MnO_x "nanoflowers" were distributed on the surface of each individual MHCF cubes, creating

a far more pronounced synergistic effect between the two constituents than the dual layer approach,[35] as demonstrated in that the composite MOF–MnO_x exhibited a significant increase (threefold) in capacitance compared with pristine MOFs, proving the utility of this extremely simple method in the interesting field of MOF-based electrochemical energy storage. The potential of this approach was further demonstrated by using MOF–MnO_x material together with activated carbon as electrodes for flexible SCs, achieving the best performance in terms of specific capacitance and energy density among MOF-based flexible SCs ever reported in the literature.

The starting materials MHCF nanocubes were synthesized according to the procedures reported in our previous work.[37] The X-ray diffraction (XRD) pattern of the product (Figure S1a, Supporting Information) shows all the reflections can be indexed to the pure face-centered cubic phase of $Mn_4Fe(CN)_{62.667} \cdot 15.84H_2O$ (ICSD-151693). No peaks of other phases can be detected, and the sharp and strong peaks imply the high purity and the good crystallinity of the product. The corresponding schematic crystal structure of the unit cell is also shown in Figure S1a in the Supporting Information, which indicates that MHCF is a classical Prussian blue analogue in terms of composition and structure. It is interesting that Mn ions are located at the outside of the unit cell, which proves necessary for the introduction of MnO_x into the MHCF system. The average crystallite size is estimated to be 17 nm as calculated using the Scherrer equation. By adding NH_4F, MHCF–MnO_x was obtained. As shown in Figure S1b in the Supporting Information, the XRD pattern of the product resembles that of MHCF, indicating the product inherits the crystal structure of the pristine MHCF, with a possible amorphous or weakly crystalline coating layer of MnO_x.

Scanning electron microscopy (SEM) images were taken to characterize the morphology of MHCF and MnO_x–MHCF. The cubic structure of MHCF seems well-defined and uniform with a diameter of about 650 nm, and the surfaces of the cubes are extremely smooth (**Figure 1**a). Figure 1b–d shows the SEM images in different magnification of MHCF after adding NH_4F, featuring remarkable morphological changes on the external surfaces of MHCF cubes. The oxides on the surfaces adopt a flower-like morphology, greatly enhancing the surface area of the product.

To further probe into the morphology, transmission electron microscope (TEM) measurements were carried out for MnO_x–MHCF, manifesting the hollow nature of MHCF cubes as well as the extremely intricate and complicated detailed structure of the "flowers" (**Figure 2**a–d). According to selected area electron diffraction (SAED) patterns in the inset of Figure 2b, strong diffraction spots are observed in MHCF nanocube area (left inset), demonstrating the single crystalline nature of MHCF, whereas the single dot patterns (right inset) suggest amorphous or weakly crystalline nature of MnO_x "flowers". The intricate
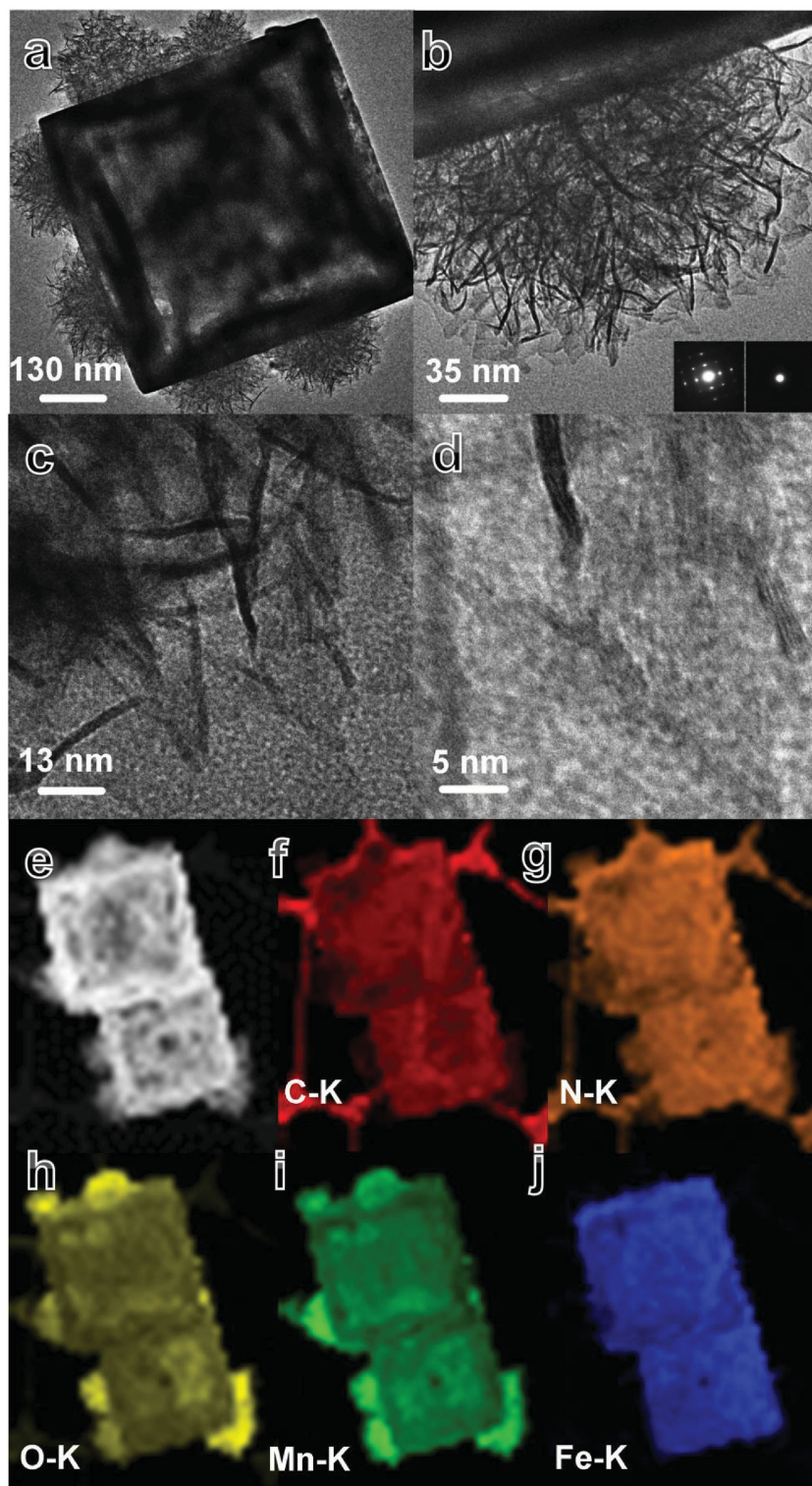
Figure 2. a–d) TEM images of MnO$_x$–MHCF at different magnification, and SAED patterns (left: nanocube, right: "flowers") in the inset of (b). e–j) EDS-mappings for different elements in MnO$_x$–MHCF.

cubes. Energy dispersive spectrometer (EDS) mapping has been measured (Figure 2e–j) to further elucidate the elemental composition of the composite material. The light intensity is proportional to the elemental content. Clearly, the flower-like structures are composed of Mn and O elements exclusively. X-ray photoelectron microscopy (XPS) measurements of MHCF (Figure S2a,b, Supporting Information) and MnO$_x$–MHCF (Figure S2c,d, Supporting Information) were conducted to study the valence states of Mn in the composite. From Figure S2a,c (Supporting Information), a broad Mn 2p3/2 peak is found around 642.3 eV, indicating the existence of a mixture of the two Mn valence states, as this value lies between the binding energy for Mn (II) and Mn (III).[38,39] By studying the Mn 3s peak, the peak separation value is found to be 5.68 eV for MHCF (Figure S2b, Supporting Information) and 5.69 eV for MnO$_x$–MHCF (Figure S2d, Supporting Information), which lie between the value for MnO (5.79–5.8 eV) and Mn$_2$O$_3$ (5.2–5.41 eV),[40,41] further implying the coexistence of the Mn (II) and Mn (III) species.

Nitrogen adsorption–desorption measurements were conducted to study the pore structures of MHCF (Figure S3a, Supporting Information) and MnO$_x$–MHCF (Figure S3b, Supporting Information). The Brunauer–Emmett–Teller (BET) surface area of MHCF and MnO$_x$–MHCF are calculated to be 512 and 818 m^2 g^{-1}, respectively. It is clear that MnO$_x$–MHCF has significantly higher specific surface than MHCF, probably due to the intricate nanostructure of MnO$_x$ "flowers". As is presented in the inset of Figure S3 (Supporting Information), the pore-size distribution of the two samples were determined with Barrett–Joyner–Halenda (BJH) method from the desorption branch of the isotherm. The average pore size of MHCF is 4 nm, whereas the pore size distribution of MnO$_x$–MHCF nanocubes center at 4 nm and 12 nm. The sharp peak at 4 nm is clearly due to MHCF, and the major broad peak centered at 12 nm is ascribed to MnO$_x$ nanoflowers, which contribute much more pore surface area than MHCF with their complicated pore structure. The hierarchical pore structure of MnO$_x$–MHCF clearly offers many more nanochannels than MHCF to contact the electrolyte through surface–interface interactions.

The electrochemical performance of MnO$_x$–MHCF electrode was studied in a three-electrode cell using 1.0 M Na$_2$SO$_4$ solution as electrolyte. The cyclic voltammetry (CV) curves of MnO$_x$–MHCF electrode at different scan rates (5–50 mV s^{-1}) (**Figure 3**a) showed

flower-like pseudocapacitive constituent provides channels for the electrolyte ions, adding to the overall capacitance due to the uniform, easily-packed-up and hollow nature of MHCF
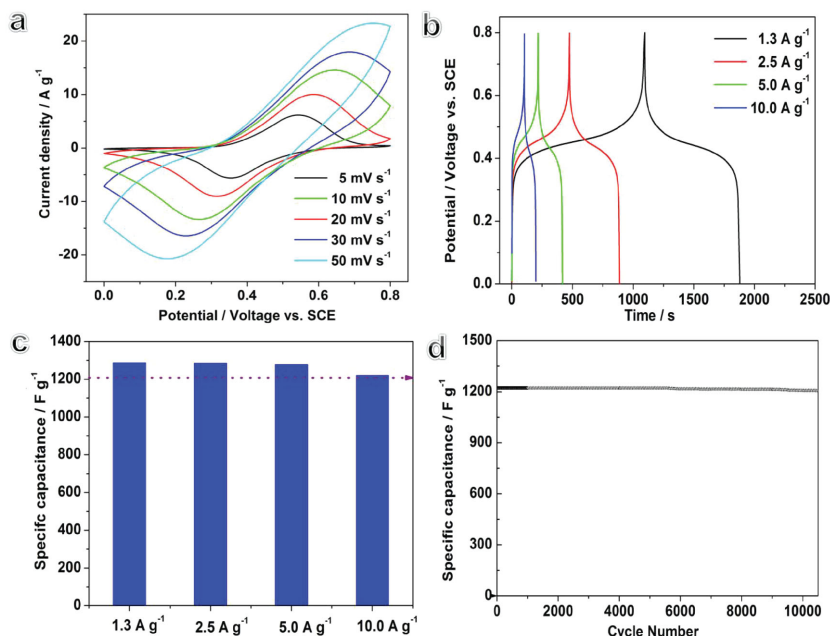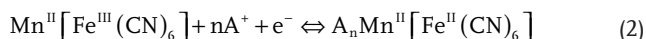
Figure 3. a) Cyclic voltammogram curves of MnO_x–MHCF electrode at different scan rates in the range of 5–50 mV s^{-1}. b) The galvanostatic charge–discharge curves of MnO_x–MHCF electrode at current densities of 1.3–10.0 A g^{-1} in 1.0 M Na_2SO_4 solution. c) Specific capacitances of MnO_x–MHCF nanocube electrodes derived from the discharging curves at the current density of 1.3–10.0 A g^{-1} in 1.0 M Na_2SO_4 solution. d) Cycling performance of the MnO_x–MHCF nanocube electrode measured at the current density of 10.0 A g^{-1} in 1.0 M Na_2SO_4 solution for 10 000 cycles .

characteristic pseudocapacitive type capacitance, adding greatly to the EDLC type capacitance endowed by MHCF. Based on the composition of the material, the pair of redox peaks within the range of 0–0.8 V come largely from the pseudocapacitance generated by faradic redox reactions of mixed-valence MnO_x and MHCF nanocubes. The reactions are as follows

$$Mn(III) \Leftrightarrow Mn(II) + e^- \tag{1}$$

$$Mn^{II}\left[Fe^{III}(CN)_6\right] + nA^+ + e^- \Leftrightarrow A_n Mn^{II}\left[Fe^{II}(CN)_6\right] \tag{2}$$

Where A represents alkali metal ions from the electrolyte.

The chronopotentiometry (CP) curves at different current densities (Figure 3b) were highly symmetric showing the outstanding reversibility of redox reactions in the electrode. From the discharge curve, we calculated the specific capacitance of MnO_x–MHCF to be ≈1200 F g^{-1} based on the total mass loading of the electrode material as shown in Figure 3c, which was four times that of the pristine MHCF tested under the same experimental setting (≈300 F g^{-1} at 10 A g^{-1}, Figure S4, Supporting Information). Moreover, the capacitance of MnO_x–MHCF remained almost the same under different current density, whereas the capacitance of MHCF decreased rapidly with the increase of the current density, showing the good rate performance of MnO_x–MHCF composite. The electrochemical performance of MnO_x–MHCF was also compared to MnO_x ultrathin nanosheets (Figure S5, Supporting Information). The electrochemical properties of MnO_x (Figure S6, Supporting

Information) were studied under the same conditions as with MnO_x–MHCF and MHCF. At the current density of 10 A g^{-1}, the specific capacitance of MnO_x–MHCF, MnO_x, and MHCF are 1200, 300, and 400 F g^{-1}, respectively, showing obvious synergistic effect of the MnO_x–MHCF composite resulting from the unique structure and the intimate contact between MHCF and MnO_x.

The capacitance is larger than most MOF-based materials ever reported so far.[42,43] Other than boosted capacitance, the in situ transformation methodology also endows the composite electrode materials (compared with MnO_x) with better conductivity possibly due to the intimate contact of the two constituents as well as good electrical conductivity of MHCF (Figure S7, Supporting Information). It is very important for electrode materials to have good cycling stability which is necessary for the SC device to work steadily and safely in the long term. As shown in Figure 3d, MnO_x–MHCF nanocube electrode retained more than 94.7% of its initial capacitance after 10 000 cycles at 10 A g^{-1}.

To further investigate the MnO_x–MHCF material for practical applications, especially for flexible energy storage, a flexible solid-state-hybrid-supercapacitor (SSHC) device was fabricated based on MnO_x–MHCF and activated carbon as active materials for the two electrodes, Pt-coated polyethylene terephthalate (PET) substrate as the flexible conductive substrate, and PVA/KOH gel electrolyte as the solid electrolyte. The fabricated devices were studied in a two electrode system. As shown in **Figure 4**a, the charge/discharge curves at different current densities of MnO_x–MHCF electrode has a small "IR drop" that indicates a small internal resistance. Areal capacitance is more relevant in the case of flexible/wearable energy storage devices, thus we calculated from the discharge curves the areal capacitance of the devices under different current density from 0.5 to 5.0 mA cm^{-2}. The maximum areal capacitances were 175, 162, 152, 142, and 127 mF cm^{-2} at the current density ranging from 0.5 to 5.0 mA cm^{-2}, which are significantly superior to results from recent reports on state-of-the-art flexible supercapacitors (Table S1, Supporting Information).[36,44–49] In addition to enhanced capacitance, the increased conductivity of the electrode also contributes to the outstanding performance of the device, as shown in the Nyquist plots for the devices made with MHCF and MHCF–MnO_x as the electrode materials (Figure S8, Supporting Information).

To test the flexibility of the device, we conducted CV tests under different bending angles (Figure 4c). In the process, the CV curves did not show noticeable changes even bending to 180°, indicating good electrochemical stability of the SC under bending conditions. In addition, the device showed a capacitance retention of ≈94.5% after 10 000 cycles at 5.0 mA cm^2, demonstrating the outstanding stability of the device in terms of long-term cycling. Furthermore, the device is so lightweight
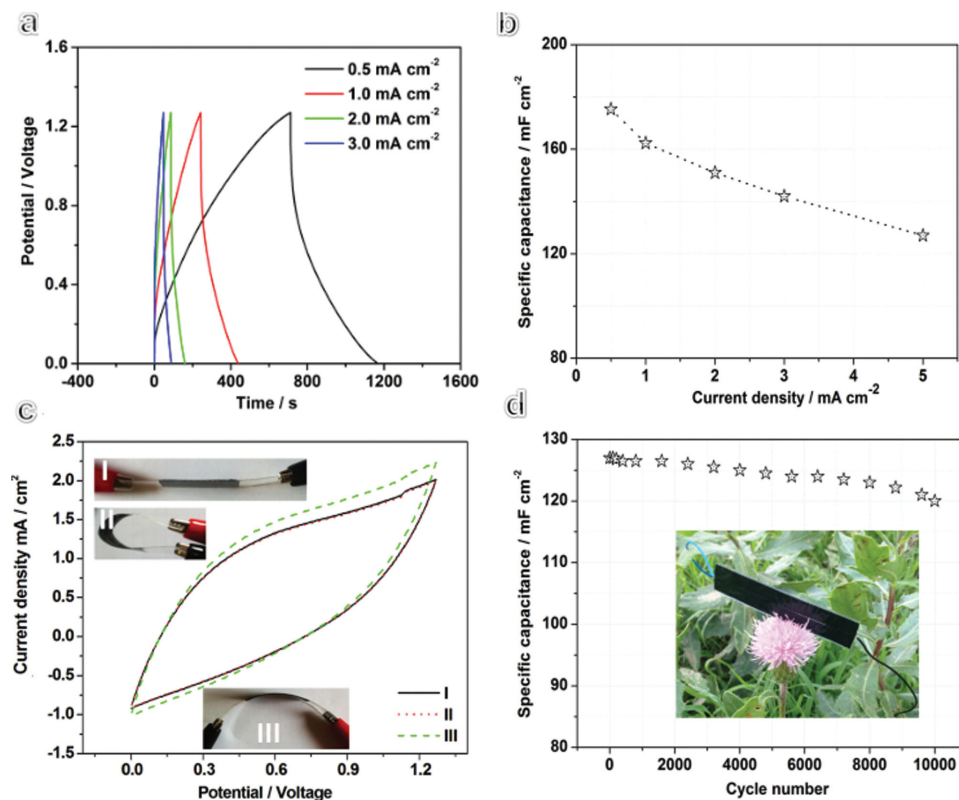
Figure 4. Electrochemical performance of a flexible supercapacitor based on MnO_x–MHCF (positive) and activated carbon (negative) active materials. a) Galvanostatic charge–discharge curves. b) Specific capacitances as a function of current density calculated from discharge curves. c) CV curves of the device under different bending angles. I: 0°; II: 90°; III: 180°. d) Cycling performance measured by charging and discharging the electrode at 5.0 mA cm^{-2} for 10 000 cycles.

that the full device can be held by the petals of a blossoming flower, showing its potential for wearable electronic applications (Figure 4d). Besides bending flexibility, the environmental stability of the device was also studied by first exposing the device to different load pressures. The device showed negligible difference in CV curves under different load pressure from weights varying from 5 g to 50 g (Figure S9, Supporting Information). The device was also subjected to different temperature (from room temperature to 90 °C (Figure S10, Supporting Information). The capacitance increased (inferred from the area under the CV curve) at 45 °C, while decreased to the base value (at room temperature) at 90 °C. The reason might be the increased ion transport behavior at elevated temperature. When further increasing the temperature, the stability of the solid electrolyte might be compromised due to the evaporation of water.

The volumetric energy and power densities of the as-prepared flexible SSHC calculated based on the data in Figure 4a are shown in **Figure 5**. For comparison, the volumetric power and energy densities of other recently reported electrochemical energy storage devices with similar structure are also plotted. The as-fabricated flexible SSHC possessed a maximum volumetric energy density of 5.1 mW h cm^{-3} (210 W h kg^{-1}). Moreover, the maximum volumetric energy density of the as-prepared flexible SSHC ranks as one of the best among recently reported flexible supercapacitors,[50–63] such as

$TiO_2@MnO_2//TiO_2@C$ (0.30 mWh cm^{-3}, 0.5 mA cm^{-2}),[51] ZnO@MnO//Graphene (0.234 mWh cm^{-3}, 0.5 mA cm^{-2}),[59] $MnO_2//Fe_2O_3$ (0.41 mWh cm^{-3}, 0.5 mA cm^{-2}),[60] polypyrrole (PPy)@layered double hydroxide (LDH)//reduced graphene oxides (rGO) (46 Wh kg^{-1}, 2 mA cm^{-2}),[53] carbon nanotubes
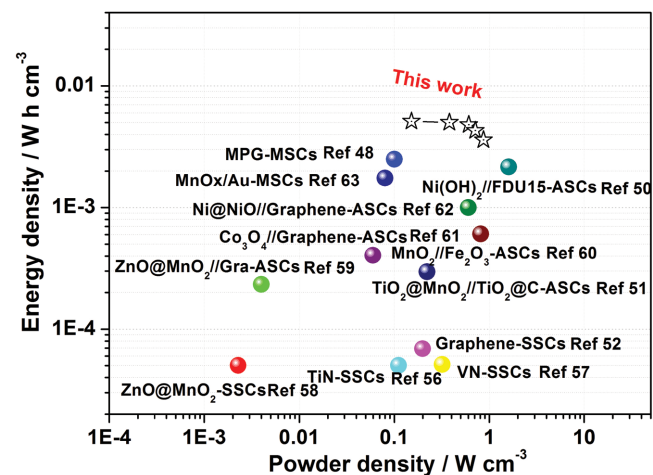

Figure 5. Ragone plots of the as-prepared SSHC device. The values reported for other state-of-the-art flexible supercapacitor devices are added for comparison.[50–63] Inset shows a red LED (1.5 V) powered by the as-prepared SSHC.

(CNTs)//Fe_3O_4-C (1.56 mWh cm^{-3}, 1.3 mA cm^{-2}),[54] and V_2O_5-electrospun carbon nanofiber (ECF)//ECF (22.3 Wh kg^{-1}, 0.3 A g^{-1}).[55] The SSHC device can power a red light-emitting-diode (LED, 1.5 V) for 2 min after being charged at 0.5 mA cm^{-2} for 30 s as shown in the inset of Figure 5.

In summary, we have developed an extremely simple in situ self-transformation method to significantly boost the electrochemical performance of MOFs including threefold increase in capacitance as well as much better rate performance. Furthermore, the obtained MnO$_x$–MHCF composite material showed great promise for flexible energy storage: A solid-state flexible SC was fabricated based on MnO$_x$–MHCF and activated carbon, and an areal capacitance of 175 mF cm^{-2} at 0.5 mA cm^{-2} was achieved. It is worthwhile to mention that the performance in this report is the best among MOF-based flexible SCs, and is among the best results among flexible SCs in general in terms of specific capacitance and energy density. Bearing all the results in mind, our simple approach has clearly provided an important insight into the rational design and synthesis of MOF-based materials for electrochemical applications such as batteries and SCs.

Experimental Section

Synthesis of MHCF Nanocubes: MHCF nanocubes were synthesized via a simple chemical precipitation method according to our previous report.[30] Briefly, 0.30 g polyvinylpyrrolidone (PVP) was dissolved in the mixed solvent system with 10 mL C_2H_5OH and 10 mL H_2O; then 0.045 g MnSO$_4\cdot$H$_2O$ was added into the above solution. At the same time, 0.066 g K$_3$Fe(CN)$_6$ was dissolved in 10 mL of distilled water. These two solutions were mixed and stirred violently for 60 min at room temperature, then the resulting black-gray mixture was filtered and washed several times with absolute ethanol and dried at room temperature.

Synthesis of MnO$_x$–MHCF Nanocubes: 0.033 g MHCF was dissolved in the mixed solvent system with 10 mL C_2H_5OH and 15 mL H_2O under stirring to get a homogeneous solution. At the same time, 0.502 g NH$_4$F was dissolved in 5 mL distilled water. Then, the obtained NH$_4$F solution was added into the MHCF solution. The obtained mixture was stirred for 20 min. The obtained product was filtered and washed several times with H_2O and CH_3CH_2OH.

Characterization: The morphology of the as-prepared samples was observed with a JEOL JSM-6701F field-emission SEM at an acceleration voltage of 5.0 kV. The phase analyses of the samples were performed by XRD on a Rigaku-Ultima III with Cu Kα radiation (λ = 1.5418 Å). TEM images were captured on a JEM-2100 microscope at an acceleration voltage of 200 kV. Nitrogen adsorption–desorption measurements were performed on a Gemini VII 2390 analyzer at 77 K using the volumetric method. The specific surface area was obtained from the N$_2$ adsorption–desorption isotherms and was calculated by the BET method.

Fabrication and Electrochemical Study on MnO$_x$–MHCF Nanocube Electrode in a Three-Electrode System: All electrochemical performances were carried out in a conventional three-electrode system with a platinum electrode and a saturated calomel electrode as the counter and reference electrodes, respectively. Before electrochemical measurements, O$_2$ was purged out from the solution by inert gas-Ar. The working electrode was made by mixing MnO$_x$–MHCF nanocubes, acetylene black, and polytetrafluoroethylene at a weight ratio of 80:15:5. The slurry was coated on a piece of foamed nickel foam ($\approx$1 cm^2), which was then pressed into a thin foil at a pressure of 5.0 MPa. The typical mass loading of the electrode material was 5.0 mg. The electrolyte was 1.0 M Na$_2$SO$_4$ solution. CV measurements of MnO$_x$–MHCF nanocube electrodes were conducted using PARSTAT2273. Galvanostatic charge–discharge

methods were used to investigate capacitive properties of MnO$_x$–MHCF nanocube electrodes, which were all carried out with an CHI-660b electrochemical instrument.

Fabrication and Electrochemical Study of Flexible MnO$_x$–MHCF/ Activated Carbon SSHC: A film of PET was used as the flexible substrate. A layer of Pt film ($\approx$3–5 nm thick) was deposited as the current collector for electrode materials. Subsequently, the slurry containing the active materials (MnO$_x$–MHCF or activated carbon) was coated on the Pt-PET, and the electrode was then used as the working electrode after drying. The mass ratio between the positive (MnO$_x$–MHCF) and negative (activated carbon) active material was 1:6. In the meantime, the PVA/KOH gel electrolyte was prepared as follows: 1.52 g PVA, 2.13 g KOH, and 15 mL DI water were mixed thoroughly at 75 °C for 30 min under vigorous stirring. Subsequently, the positive and negative electrodes were immersed in the PVA/KOH gel solution for $\approx$5–10 min to be covered with a layer of solid electrolytes. After the excess water was vaporized, the two electrodes were pressed together on a sheet out roller. Thus, a stacked device was fabricated. CV measurements were conducted on PARSTAT-2273. The flexible MnO$_x$–MHCF//Active carbon devices were galvanostatically charged and discharged at the current density of 0.5–5.0 mA cm^{-2} on the Arbin-BT6000 electrochemical instrument. All the electrochemical measurements were conducted at room temperature.

Supporting Information

Supporting Information is available from the Wiley Online Library or from the author.

Acknowledgements

[1] S. Chu, A. Majumdar, *Nature* **2012**, *488*, 294.
[2] A. Nathan, A. Ahnood, M. T. Cole, L. Sungsik, Y. Suzuki, P. Hiralal, F. Bonaccorso, T. Hasan, L. Garcia-Gancedo, A. Dyadyusha, S. Haque, P. Andrew, S. Hofmann, J. Moultrie, C. Daping, A. J. Flewitt, A. C. Ferrari, M. J. Kelly, J. Robertson, G. Amaratunga, W. I. Milne, *Proc. IEEE* **2012**, *100*, 1486.
[3] Z. Liu, J. Xu, D. Chen, G. Shen, *Chem. Soc. Rev.* **2015**, *44*, 161.
[4] Y. Z. Zhang, Y. Wang, T. Cheng, W. Y. Lai, H. Pang, W. Huang, *Chem. Soc. Rev.* **2015**, *44*, 5181.

COMMUNICATION

[5] D. Yu, Q. Qian, L. Wei, W. Jiang, K. Goh, J. Wei, J. Zhang, Y. Chen, *Chem. Soc. Rev.* **2014**, *44*, 647.

[6] P. Simon, Y. Gogotsi, *Nat. Mater.* **2008**, *7*, 845.

[7] X. Peng, L. Peng, C. Wu, Y. Xie, *Chem. Soc. Rev.* **2014**, *43*, 3303.

[8] J. Yan, Q. Wang, T. Wei, Z. Fan, *Adv. Energy Mater.* **2014**, *4*, 1300816.

[9] Z. Yu, L. Tetard, L. Zhai, J. Thomas, *Energy Environ. Sci.* **2015**, *8*, 702.

[10] P. Yang, W. Mai, *Nano Energy* **2014**, *8*, 274.

[11] S. Y. Lee, K. H. Choi, W. S. Choi, Y. H. Kwon, H.-R. Jung, H.-C. Shin, J. Y. Kim, *Energy Environ. Sci.* **2013**, *6*, 2414.

[12] L. L. Zhang, X. S. Zhao, *Chem. Soc. Rev.* **2009**, *38*, 2520.

[13] N. A. Choudhury, S. Sampath, A. K. Shukla, *Energy Environ. Sci.* **2009**, *2*, 55.

[14] H. Tang, J. Wang, H. Yin, H. Zhao, D. Wang, Z. Tang, *Adv. Mater.* **2015**, *27*, 1117.

[15] H. Wang, Z. Xu, H. Yi, H. Wei, Z. Guo, X. Wang, *Nano Energy* **2014**, *7*, 86.

[16] S. Zhao, Y. Li, H. Yin, Z. Liu, E. Luan, F. Zhao, Z. Tang, S. Liu, *Sci. Adv.* **2015**, *1*, e1500372.

[17] H. Xia, C. Hong, B. Li, B. Zhao, Z. Lin, M. Zheng, S. V. Savilov, S. M. Aldoshin, *Adv. Funct. Mater.* **2015**, *25*, 627.

[18] H. Li, M. Eddaoudi, M. O'Keeffe, O. M. Yaghi, *Nature* **1999**, *42*, 276.

[19] B. Li, H.-M. Wen, W. Zhou, B. Chen, *J. Phys. Chem. Lett.* **2014**, *5*, 3468.

[20] K. Na, K. M. Choi, O. M. Yaghi, G. A. Somorjai, *Nano Lett.* **2014**, *14*, 5979.

[21] S. Zhao, H. Yin, L. Du, L. He, K. Zhao, L. Chang, G. Yin, H. Zhao, S. Liu, Z. Tang, *ACS Nano* **2014**, *8*, 12660.

[22] P. Horcajada, T. Chalati, C. Serre, B. Gillet, C. Sebrie, T. Baati, J. F. Eubank, D. Heurtaux, P. Clayette, C. Kreuz, J.-S. Chang, Y. K. Hwang, V. Marsaud, P.-N. Bories, L. Cynober, S. Gil, G. Ferey, P. Couvreur, R. Gref, *Nat. Mater.* **2010**, *9*, 172.

[23] B. Chen, L. Wang, F. Zapata, G. Qian, B. E. Lobkovsky, *J. Am. Chem. Soc.* **2008**, *130*, 6718.

[24] L. He, Y. Liu, J. Liu, Y. Xiong, J. Zheng, Y. Liu, Z. Tang, *Angew. Chem., Int. Ed.* **2013**, *52*, 3741.

[25] S. Bhattacharyya, A. Chakraborty, K. Jayaramulu, A. Hazra, T. K. Maji, *Chem. Commun.* **2014**, *50*, 13567.

[26] B. Liu, H. Shioyama, T. Akita, Q. Xu, *J. Am. Chem. Soc.* **2008**, *130*, 5390.

[27] J. W. Jeon, R. Sharma, P. Meduri, B. W. Arey, H. T. Schaef, J. L. Lutkenhaus, J. P. Lemmon, P. K. Thallapally, M. I. Nandasiri, B. P. McGrail, S. K. Nune, *ACS Appl. Mater. Interfaces* **2014**, *6*, 7214.

[28] R. R. Salunkhe, Y. Kamachi, N. L. Torad, S. M. Hwang, Z. Sun, S. X. Dou, J. H. Kim, Y. Yamauchi, *J. Mater. Chem. A* **2014**, *2*, 19848.

[29] N. L. Torad, R. R. Salunkhe, Y. Li, H. Hamoudi, M. Imura, Y. Sakka, C. C. Hu, Y. Yamauchi, *Chem.- Eur. J.* **2014**, *20*, 7895.

[30] J. Tang, R. R. Salunkhe, J. Liu, N. L. Torad, M. Imura, S. Furukawa, Y. Yamauchi, *J. Am. Chem. Soc.* **2015**, *137*, 1572.

[31] F. Meng, Z. Fang, Z. Li, W. Xu, M. Wang, Y. Liu, J. Zhang, W. Wang, D. Zhao, X. Guo, *J. Mater. Chem. A* **2013**, *1*, 7235.

[32] W. Meng, W. Chen, L. Zhao, Y. Huang, M. Zhu, Y. Huang, Y. Fu, F. Geng, J. Yu, X. Chen, C. Zhi, *Nano Energy* **2014**, *8*, 133.

[33] K. M. Choi, H. M. Jeong, J. H. Park, Y.-B. Zhang, J. K. Kang, O. M. Yaghi, *ACS Nano* **2014**, *8*, 7451.

[34] P. C. Banerjee, D. E. Lobo, R. Middag, W. K. Ng, M. E. Shaibani, M. Majumder, *ACS Appl. Mater. Interfaces* **2015**, *7*, 3655.

[35] Y. Wang, Q. Chen, *ACS Appl. Mater. Interfaces* **2014**, *6*, 6196.

[36] L. Wang, X. Feng, L. Ren, Q. Piao, J. Zhong, Y. Wang, H. Li, Y. Chen, B. Wang, *J. Am. Chem. Soc.* **2015**, *137*, 4920.

[37] H. Pang, Y. Z. Zhang, T. Cheng, W. Y. Lai, W. Huang, *Nanoscale* **2015**, *7*, 16012.

[38] J.-K. Chang, W.-T. Tsai, *J. Appl. Electrochem.* **2004**, *34*, 953.

[39] C.-C. Hu, C.-C. Wang, *J. Appl. Electrochem.* **2003**, *150*, A1079.

[40] M. Chigane, M. Ishikawa, *J. Appl. Electrochem.* **2000**, *147*, 2246.

[41] M. Chigane, M. Ishikawa, M. Izaki, *J. Appl. Electrochem.* **2001**, *148*, D96.

[42] R. R. Salunkhe, J. Tang, Y. Kamachi, T. Nakato, J. H. Kim, Y. Yamauchi, *ACS Nano* **2015**, *9*, 6288.

[43] J. Yang, P. Xiong, C. Zheng, H. Qiu, M. Wei, *J. Mater. Chem. A* **2014**, *2*, 16640.

[44] X. Pu, L. Li, M. Liu, C. Jiang, C. Du, Z. Zhao, W. Hu, Z. L. Wang, *Adv. Mater.* **2015**, *27*, 2472.

[45] F. H. Su, X. M. Lv, M. H. Miao, *Small* **2015**, *11*, 854.

[46] Y. N. Meng, Y. Zhao, C. G. Hu, H. H. Cheng, Y. Hu, Z. P. Zhang, G. Q. Shi, L. T. Qu, *Adv. Mater.* **2013**, *25*, 2326.

[47] C. Z. Wu, X. L. Lu, L. L. Peng, K. Xu, X. Peng, J. L. Huang, G. H. Yu, Y. Xie, *Nat. Commun.* **2013**, *4*, 2431.

[48] Z. S. Wu, K. Parvez, X. Feng, K. Müllen, *Nat. Commun.* **2013**, *4*, 2487.

[49] L. Kou, T. Huang, B. Zheng, Y. Han, X. Zhao, K. Gopalsamy, H. Sun, C. Gao, *Nat. Commun.* **2014**, *5*, 3754.

[50] X. L. Dong, Z. Y. Guo, Y. F. Song, M. Y. Hou, J. Q. Wang, Y. G. Wang, Y. Y. Xia, *Adv. Funct. Mater.* **2014**, *24*, 3405.

[51] X. H. Lu, M. H. Yu, G. M. Wang, T. Zhai, S. L. Xie, Y. C. Ling, Y. X. Tong, Y. Li, *Adv. Mater.* **2013**, *25*, 267.

[52] M. F. El-Kady, V. Strong, S. Dubin, R. B. Kaner, *Science* **2012**, *335*, 1326.

[53] M. Shao, Z. Li, R. Zhang, F. Ning, M. Wei, D. G. Evans, X. Duan, *Small* **2015**, *11*, 3530.

[54] R. Li, Y. Wang, C. Zhou, C. Wang, X. Ba, Y. Li, X. Huang, J. Liu, *Adv. Funct. Mater.* **2015**, *25*, 5384.

[55] L. Li, S. Peng, H. B. Wu, L. Yu, S. Madhavi, X. W. D. Lou, *Adv. Energy Mater.* **2015**, *5*, 1500753.

[56] X. H. Lu, G. M. Wang, T. Zhai, M. H. Yu, S. L. Xie, Y. C. Ling, C. L. Liang, Y. X. Tong, Y. Li, *Nano Lett.* **2012**, *12*, 5376.

[57] X. H. Lu, M. H. Yu, T. Zhai, G. M. Wang, S. L. Xie, T. Y. Liu, C. L. Liang, Y. X. Tong, Y. Li, *Nano Lett.* **2013**, *13*, 2628.

[58] P. H. Yang, X. Xiao, Y. Z. Li, Y. Ding, P. F. Qiang, X. H. Tan, W. J. Mai, Z. Y. Lin, W. Z. Wu, T. Q. Li, H. Y. Jin, P. Y. Liu, J. Zhou, C. P. Wong, Z. L. Wang, *ACS Nano* **2013**, *7*, 2617.

[59] Z. L. Wang, Z. Zhu, J. Qiu, S. Yang, *J. Mater. Chem. C* **2014**, *2*, 1331.

[60] X. Lu, Y. Zeng, M. Yu, T. Zhai, C. Liang, S. Xie, M. S. Balogun, Y. Tong, *Adv. Mater.* **2014**, *26*, 3148.

[61] X. Wang, B. Liu, R. Liu, Q. Wang, X. Hou, D. Chen, R. Wang, G. Shen, *Angew. Chem. Int. Ed.* **2014**, *126*, 1880.

[62] M. Yu, W. Wang, C. Li, T. Zhai, X. Lu, Y. Tong, *NPG Asia Mater.* **2014**, *6*, e129.

[63] W. Si, C. Yan, Y. Chen, S. Oswald, L. Han, O. G. Schmidt, *Energy Environ. Sci.* **2013**, *6*, 3218.